JCTC Journal of Chemical Theory and Computation

ARTICLE

pubs.acs.org/JCTC

Dual Fluorescence of Fluorazene in Solution: A Computational Study

Ignacio Fdez. Galván,* M. Elena Martín, Aurora Muñoz-Losa, and Manuel A. Aguilar

Química Física, Edif. José María Viguera Lobo, Universidad de Extremadura, Avda. de Elvas s/n, 06071 Badajoz, Spain

ABSTRACT: The fluorazene molecule presents dual fluorescence in polar solvents. Its absorption and emission properties in gas phase and in acetonitrile solution have been studied theoretically using the complete active space second-order perturbation//complete active space self-consistent field quantum methodology and average solvent electrostatic potential from molecular dynamics for the solvent effects. In gas phase, two optimized excited-state geometries were obtained, one of them corresponds to a local excitation (LE), and the other is an intramolecular charge transfer (ICT) and lies higher in energy. In acetonitrile solution, a second ICT structure where the molecule remains planar is found, and the energy differences are reduced. Fluorescence energies from LE and the planar ICT have a good agreement with the experimental bands, but emission from the bent ICT has too low an energy.

1. INTRODUCTION

A significant number of organic molecules with electron-donating and -withdrawing groups when immersed in polar solvents display what is known as dual fluorescence. In nonpolar solvents, as for most molecules, the fluorescence spectrum exhibits a single band, whose maximum is only slightly shifted as the solvent polarity increases, this is called the "normal" band. In polar solvents, a second fluorescence band appears in the spectrum, and the position of this second band varies more significantly with the solvent polarity, this is called the "anomalous" band. The relative intensity of the anomalous band increases with the polarity, so that in highly polar solvents, the normal band can disappear, and only the anomalous band is observed. This dual fluorescence phenomenon has been profusely studied in the literature since its discovery half a century ago.[1,2] Most of these studies are focused on the prototype molecule 4-(*N*,*N*-dimethylamino)benzonitrile (DMABN) or its derivatives, including experimental investigations[3−8] and theoretical works.[9−16] It was suggested early on that the origin of the anomalous fluorescence band is the existence of an intramolecular charge transfer (ICT) excited state, which is not normally accessible in nonpolar solvents but which is stabilized in polar solvents and can thus compete with the state responsible for the normal band, usually called a local excitation (LE) state.

The validity of this explanation for the dual fluorescence is still generally accepted. There is, however, a continuing controversy between the various groups that have investigated this subject, regarding the nature and the geometry of the ICT state, the mechanism through which the LE and ICT states are formed, the possible existence of further intermediate states, and practically every other detail of the dual fluorescence phenomenon.

Probably the most accepted models for the dual fluorescence in the DMABN molecule, and related compounds are the ones known as twisted ICT (TICT) and planar ICT (PICT). These models propose an ICT state where the donor and acceptor groups adopt, respectively, a perpendicular or coplanar conformation. Experimental evidence favoring one model or the other is usually derived from comparison of the properties of compounds with different geometric constraints and substituents. For example, compounds, like 3,5-dimethyl-4-(*N*,*N*-dimethylamino)benzonitrile, where the dimethylamino group is forced to be twisted, display only the ICT band in fluorescence, suggesting a TICT is responsible for the band. Other compounds where the twisting is hindered (like 6-cyano-1,2,3,4-tethrahydroquinoline, NTC6) can present dual fluorescence, which points to a PICT state. These apparently contradictory conclusions possibly indicate that the two models are not exclusive, and each particular system will favor one of them.

In recent years, a pair of closely related molecules has been studied for their dual fluorescence properties, see Figure 1. The two rings in 1-phenylpyrrole (PP) can freely rotate around the middle bond, while the methylene bridge in fluorazene (FPP) effectively locks the rings in an almost planar conformation. Both molecules display a very similar photophysical behavior, and in particular, both show dual fluorescence in polar solvents. One of the differences between the two molecules is that apparently FPP presents enhanced ICT emission compared to PP: the ICT band appears in less polar solvents, and its quantum yield is higher. This fact naturally leads to the conclusion that the PICT model applies better to these molecules.[17,18] However, most theoretical calculations predict a twisted structure for the ICT state of PP,[19−23] which seems unsatisfactory.

In a previous work,[24] we carried out a theoretical study on the absorption and fluorescence properties of the PP molecule, both in the gas phase and in acetonitrile solution. Our conclusion was that there are different molecular structures accessible for the PP and that the twisting of the rings is not necessary for reaching the emitting ICT state. In this work we present a similar study for the FPP molecule, where its electronic states are described with a multiconfigurational quantum method, and we used an explicit model of atomic detail for the solvent. By examining the relative energies, geometries, and emission energies of the different electronic states, we expect to obtain meaningful conclusions for the study of this system.

Received: July 28, 2011
Published: September 27, 2011

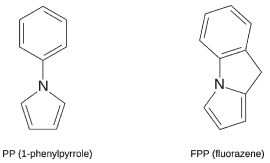

Figure 1. Two related compounds with dual fluorescence.

2. METHODS AND DETAILS

Solvent effects on the FPP UV−vis spectra were calculated with the average solvent electrostatic potential from molecular dynamics (ASEP/MD) method. This is a sequential quantum mechanics/molecular mechanics (QM/MM) method implementing the mean field approximation. It combines, alternately, a high-level QM description of the solute with a classical MM description of the solvent. One of its main features is the fact that the solvent effect is introduced into the solute's wave function as an average perturbation. Details of the method have been described in previous papers,[25−27] so here we will only present a brief outline.

As mentioned above, ASEP/MD is a method combining QM and MM techniques, with the particularity that full QM and molecular dynamics (MD) calculations are alternated and not simultaneous. During the MD simulations, the intramolecular geometry and charge distribution of all molecules are considered fixed. From the resulting simulation data, the average electrostatic potential generated by the solvent on the solute (ASEP) is obtained. This potential is introduced as a perturbation into the solute's quantum mechanical Hamiltonian, and by solving the associated Schrödinger equation, one gets a new charge distribution for the solute, which is used in the next MD simulation. This iterative process is repeated until the electron distribution of the solute and the solvent structure around it are mutually equilibrated.

The ASEP/MD framework can also be used to optimize the geometry of the solute molecule.[28] At each step of the ASEP/MD procedure, the gradient and Hessian on the system's free energy surface (including the van der Waals contribution) can be obtained, and thus they can be used to search for stationary points on this surface by some optimization method. In the computation of the gradient and Hessian, the free energy gradient method[29] is used, with the incorporation of the mean field approximation to reduce the number of quantum calculations needed. In this way, after each MD simulation, the solute geometry is optimized within the fixed "average" solvent structure by using the free energy derivatives. In the next MD simulation, the new solute geometry and charge distribution are used. This approach allows the optimization of the solute geometry in parallel to the solvent structure.

For calculating transition energies, nonequilibrium solvation is assumed. The iterative process is only performed on the initial state of the transition (the ground state for absorption, the excited state for emission), i.e., the atomic charges for the MD and the energy derivatives for the geometry optimization of the solute are calculated with the initial state's wave function. Then, with a frozen solvent model, the energies of the final states are obtained.

Once the different solute electronic states and the solvent structure around them have been optimized and equilibrated, the free energy differences between those states can be calculated, within the ASEP/MD framework, making use of the free energy perturbation method.[30,31] The expression we use to calculate the free energy difference between two species in equilibrium in solution, ΔG, is

$$\Delta G = \Delta E + \Delta G_{\text{int}} + \Delta V \quad (1)$$

where ΔE is the difference in the internal quantum energy of the solute between the two species, ΔG_{int} is the difference in the solute−solvent interaction energy, which is calculated classically with the free energy perturbation (FEP) method, and ΔV is a term that includes the difference in the zero point energy and entropic contributions of the solute. The last term, ΔV, is normally evaluated by applying the harmonic approximation to the vibrational modes of the solute in solution, and it needs the information provided by the Hessian matrix. In this work, obtaining an accurate enough Hessian matrix required computational resources that were too large, and we decided to approximate the results by neglecting this term. It must be noted that this ΔV term refers only to the internal nuclear degrees of freedom of the solute; free energy contributions from the solvent around the solute are properly accounted for in the ΔG_{int} term.

2.1. Computational Details. The quantum calculations on the solute molecule were done with the complete active space self-consistent field (CASSCF) method,[32] using the cc-pVDZ basis set and aug-cc-pVDZ in some selected cases. The active orbitals were the 6 π and π^* valence orbitals of the phenyl ring, plus the 5 π and π^* of the pyrrole ring, and 12 electrons were included in these orbitals, for a (12,11) total active space. All calculations were performed using a state average (SA) of the first five singlet states, with equal weights. It is known that, in order to obtain accurate transition energies, it is necessary to include the dynamic electron correlation in the quantum calculations, which we did with the complete active space second order perturbation (CASPT2) method,[33,34] using the SA(5)-CASSCF(12,11) wave functions as a reference. An ionization potential−electron affinity (IPEA) shifted zeroth-order Hamiltonian has been proposed for CASPT2 calculations,[35] which is supposed to reduce systematic overstabilization errors in open-shell systems (as is the case of the excited states studied here). We did all CASPT2 with the proposed IPEA shift of 0.25 E_h(CASPT2(0.25)) as well as with no IPEA shift (CASPT2(0.00)). To minimize the appearance of intruder states, an additional imaginary shift of 0.1 iE_h was used. No symmetry was assumed in any case.

The MD simulations were carried out with rigid molecules, with acetonitrile (CH_3CN) as a solvent. Lennard-Jones parameters and solvent atomic charges were taken from the optimized potentials for liquid simulations, all atoms (OPLS-AA) force field,[36] solute atomic charges were calculated from the quantum calculations through a least-squares fit to the electrostatic potential obtained at the points where the solvent charges are located. The geometry of acetonitrile was optimized with Becke's three-parameter Lee−Yang−Parr density functional (B3LYP) and the 6-311G** basis set. A total of 375 CH_3CN molecules and the solute were included at the experimental solvent density (779.3 kg/m^3). Periodic boundary conditions were applied, and spherical cutoffs were used to truncate the interatomic interactions at 12.75 Å. Long-range interactions were calculated using the Ewald sum technique. The temperature was fixed at 298.15 K by using the Nosé−Hoover thermostat. A time step of 0.5 fs was used during the simulations, and each one was run for 50 ps after 25 ps of equilibration.

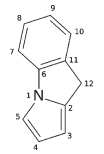

Figure 2. Atom numbering of the FPP molecule.

Table 1. Definition of geometric parameters for the FPP molecule. *d* is a bond length, *a* a bond angle, and *D* a dihedral angle. Point A is placed at $C_6 + n(Ph)$, where $n(Ph)$ is the normal vector of the best-fit plane for the phenyl carbon atoms, except C_6. Point B is defined similarly for the N1 atom and the pyrrole ring (including the nitrogen)

$$\overline{Ph} = \frac{1}{6}(d(C_6C_7) + d(C_7C_8) + d(C_8C_9) + d(C_9C_{10}) + d(C_{10}C_{11}) + d(C_{11}C_6))$$

$$\overline{Py} = \frac{1}{5}(d(N_1C_2) + d(C_2C_3) + d(C_3C_4) + d(C_4C_5) + d(C_5N_1))$$

$$Q(Ph) = \frac{1}{4}(d(C_6C_7) + d(C_8C_9) + d(C_9C_{10}) + d(C_{11}C_6)) - \frac{1}{2}(d(C_7C_8) + d(C_{10}C_{11}))$$

$$Q'(Ph) = \frac{1}{4}(d(C_6C_7) + d(C_7C_8) + d(C_9C_{10}) + d(C_{10}C_{11})) - \frac{1}{2}(d(C_8C_9) + d(C_{11}C_6))$$

$$Q(Py) = \frac{1}{3}(d(N_1C_2) + d(C_3C_4) + d(C_5N_1)) - \frac{1}{2}(d(C_2C_3) + d(C_4C_5))$$

$$Ph - Py = d(N_1C_6)$$

$$\phi = a(AC_6N_1) - 90°$$

$$\psi = a(BN_1C_6) - 90°$$

$$\theta = D(AC_6N_1B)$$

At each step of the ASEP/MD procedure, 500 configurations evenly distributed from the MD run were used to calculate the ASEP. The charges from each solvent molecule were kept explicitly whenever the molecule's center of mass was closer than 9 a_0 to any solute nucleus; the effect of the farther molecules was included in an additional shell of fitted charges. Each ASEP/MD run was continued until the energies and solute geometry and charges were stabilized for at least five iterations, results are reported as the average of these last five iterations.

For in solution calculations, a development version of the ASEP/MD software[26] was used. All quantum calculations were performed with Molcas-7.4.[37] All MD simulations were performed using Moldy.[38] The electrostatic potential generated by the solute was calculated with Molden.[39]

3. RESULTS AND DISCUSSION

3.1. Gas Phase. *3.1.1. Optimized Geometries.* The geometry of the FPP molecule was optimized in the gas phase at the SA(5)-CASSCF(12,11)/cc-pVDZ level for the electronic ground state and different singlet excited states. For describing and comparing the structures, we use some geometric parameters, such as the average bond length of the phenyl ring ($\overline{Ph}$), the average bond length of the pyrrole ring ($\overline{Py}$), the phenyl-pyrrole bond length (Ph−Py), or the phenyl pyrrole twist angle (θ). See Figure 2 and Table 1 for the atom numbering and parameter definitions.

Table 2. Geometrical parameters and dipole moments of the different optimized structures of FPP in the gas phase. Geometries optimized at the SA-CASSCF level, dipoles calculated at the CASPT2(0.00) level. The negative sign in the dipole indicates the negative charge is displaced toward the phenyl ring

	GS (S_0)	LE (S_1)	BQ (S_1)
$\overline{Ph}$ (Å)	1.400	1.433	1.421
$\overline{Py}$ (Å)	1.391	1.393	1.396
Q(Ph) (Å)	0.005	−0.003	0.069
Q(Py) (Å)	0.016	0.030	−0.105
Ph−Py (Å)	1.376	1.363	1.446
ϕ (°)	−0.1	0.0	30.1
ψ (°)	−0.1	0.0	−4.9
θ (°)	0.0	0.0	2.1
μ (D)	1.18	0.10	−6.33

Table 3. Vertical Absorption Energies (in eV), Dipole Moments (in D), and Oscillator Strengths For the FPP Molecule in the Gas Phase at the GS Geometry[a]

	vertical energies					
	CASSCF	CASPT2		expt[b]	μ	f
S_0					1.18	
S_1	4.63	4.64	4.26	4.22	0.09	0.013
S_2	5.75	5.18	4.68	4.71	−3.65	0.276
S_3	5.91	5.56	5.18	(5.05)	−6.12	0.028
S_4	6.21	5.69	5.23		−7.99	0.174

[a] Dipole moments and oscillator strengths calculated at the CASPT2-(0.00) level. [b] In *n*-hexane.[18]

The optimized ground state (GS) structure shows benzene and pyrrole rings with normal aromatic bond lengths ($\overline{Ph}$ = 1.400 Å, $\overline{Py}$ = 1.391 Å). The two rings are coplanar, as can be seen in the values of the angles ϕ, ψ and θ in Table 2. The bond lengths are in general agreement with other published computed values,[23,40] although our Ph−Py length, 1.376 Å, is 0.02 Å shorter than the value reported in those works. This difference is probably due to the state averaging in our calculations.

At the ground state geometry, the first excited state corresponds mainly to a $\pi \rightarrow \pi^*$ transition in the phenyl ring. Optimisation of this state leads to the LE (local excitation) geometry. In this structure the rings are also coplanar and Ph−Py is shorter than for the GS (1.363 Å). The local excitation character of this state is reflected in the significant increase of $\overline{Ph}$ to 1.433 Å. These features agree with the results of Xu et al.,[23] with about the same difference in Ph−Py as with GS. He and Li,[40] however, report a LE geometry with more important differences, which they call "quinoid-like", with a still shorter Ph−Py length (1.347 Å) and smaller $\overline{Ph}$; this might be due to their use of a reduced active space (10 electrons in 9 orbitals). The dipole moment of this state is practically zero.

The higher excited states at the GS geometry have a marked charge transfer character. The electron density polarization is inverted with respect to the ground state and the negative charge is displaced toward the phenyl ring (this change of direction in the polaraziation is indicated with a negative sign in the dipole moment values in the tables). We optimized the geometry of a

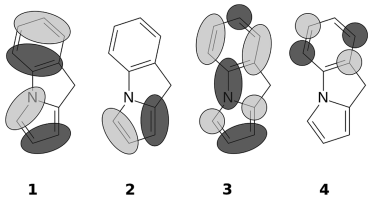

Figure 3. Main active molecular π orbitals of FPP (simplified). In the dominant ground-state configuration, orbitals 1 and 2 are doubly occupied, while 3 and 4 are empty ($1^2 2^2 3^0 4^0$).

Table 4. Vertical Emission Energies (transitions to S_0, in eV), Dipole Moments (in D), and Oscillator Strengths for the FPP Molecule in the Gas Phase[a]

	vertical energies					
	CASPT2		expt[b]	μ	f	ΔE
LE (S_1)	4.30	3.92	3.98	0.10	0.015	4.03
BQ (S_1)	3.55	3.29		−6.33	0.005	4.55

[a] ΔE is the relative energy (in eV) with respect to the ground-state minimum, GS. Dipole moments, oscillator strengths, and ΔE calculated at the CASPT2(0.00) level. [b] In *n*-hexane.[18]

charge transfer state in the gas phase, characterized by a quinoidal phenyl ring and a bend between the two aromatic rings, and therefore we will name it BQ (bent quinoidal). This structure has a pyramidalised C_6 atom, which is also displaced out of the main phenyl plane. The two rings are distorted as described by the values of Q(Ph) (positive) and Q(Py) (negative), and the Ph−Py length is significantly larger than for the GS and LE structures. Xu et al.[23] report a similar structure for the ICT minimum, but He and Li[40] give a structure with "anti-quinoidal" phenyl ring (negative Q(Ph)). We could not obtain any different ICT minimum in our calculations in the gas phase, which may be due again to the different computational level employed.

3.1.2. Absorption. The vertical absorption properties of FPP calculated at the optimized ground-state geometry (GS) are summarized in Table 3. The CASSCF transition energies are included for comparison, but it is known that dynamic electron correlation must be included to obtain reliable results, and therefore, we will only discuss CASPT2 energies in the rest of the article. By comparing the two CASPT2 columns, it is clear that CASPT2(0.25) values are consistently 0.4 eV to 0.5 eV larger than CASPT2(0.00) values, a difference that has been found and discussed in other works.[24,41−43] Other properties like dipole moments or oscillator strengths do not show such variations, and only CASPT2(0.00) values are reported for them. From the values in Table 3, the $S_0 \rightarrow S_2$ transition appears to be the most active in absorption, while the $S_0 \rightarrow S_1$ transition should be much weaker, and the $S_0 \rightarrow S_4$ transition could also be observed. The experimental absorption spectrum of FPP in *n*-hexane[18] has a strong band at 4.71 eV, a much weaker band at 4.22 eV, and a shoulder at around 5.05 eV. Although CASPT2-(0.25) results are generally less sensitive to basis set or active space changes and more similar to other methods of like quality, for the present calculations CASPT2(0.00) results are in better agreement with the experimental values. Therefore, to facilitate the discussion, in the rest of this work, we will refer in general to CASPT2(0.00) values. A single-point calculation with diffuse functions, using the aug-cc-pVDZ basis set, yielded very similar

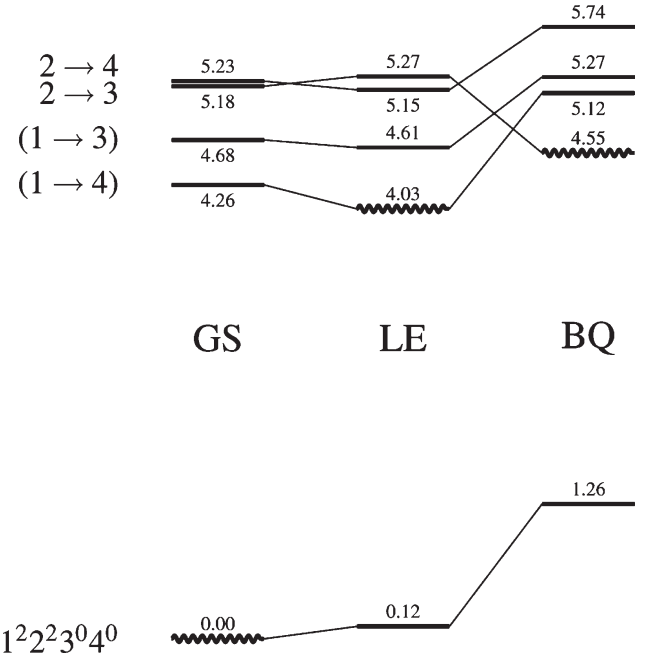

Figure 4. Relative energies (CASPT2(0.00), in eV) of the calculated electronic states of FPP in the gas phase at the optimized geometries. The state for which each geometry is optimized is drawn as a wavy line. States of equivalent electron configuration are joined by lines. For the nature of the different states, labeled on the left, refer to Table 3, Figure 3, and the corresponding text.

results, with all absorption energies 0.1 eV to 0.2 eV lower, as observed in previous works when the basis set is enlarged.

The electronic states S_3 and S_4 are dominated by single excitations from the pyrrole ring to the phenyl. In terms of the simplified molecular orbitals pictured in Figure 3, S_3 is a $2 \rightarrow 3$ transition, and S_4 is a $2 \rightarrow 4$ transition. S_1 and S_2 are not so clearly dominated by one configuration, but they have the larger contribution from $1 \rightarrow 4$ and $1 \rightarrow 3$ transitions, respectively. The electronic state optimized in the LE structure described above is equivalent to S_1, while the state optimized in the BQ ICT structure corresponds to S_3 ($2 \rightarrow 3$ transition), as suggested by the values of Q(Ph) and Q(Py).

3.1.3. Fluorescence. The fluorescence energies from the two excited states optimized in the gas phase are shown in Table 4. The predicted emission from the LE state is 0.34 eV lower that the absorption with both CASPT2 variants, this agrees fairly well with the experimental Stokes shift of 0.24 eV in *n*-hexane. As occurred in the absorption, the best agreement with the experimental fluorescence is obtained with CASPT2(0.00). The ΔE value of 4.03 eV can be compared with the experimental value obtained from the crossing point of the absorption and fluorescence spectra, which is 4.24 eV in *n*-hexane. Fluorescence at the BQ geometry is calculated to have a much lower energy (0.63 eV lower at the CASPT2(0.00) level), but the emitting state is 0.52 eV above the LE state and above the Franck−Condon S_1 state at the GS geometry. This is probably a reason why there is no observed ICT fluorescence in nonpolar solvents. A scheme of the relative energies of the electronic states at the different geometries is presented in Figure 4. Again, aug-cc-pVDZ single-point calculations give very similar result, with fluorescence energies around 0.1 eV lower in all cases.

Table 5. Geometrical Parameters and Dipole Moments of the Different Optimized Structures of FPP in Acetonitrile Solution[a]

	GS (S_0)	LE (S_1)	BQ (S_1)	LQ (S_1)
$\overline{\text{Ph}}$ (Å)	1.400	1.433	1.419	1.413
$\overline{\text{Py}}$ (Å)	1.391	1.393	1.393	1.391
Q(Ph) (Å)	0.005	−0.003	0.064	0.052[b]
Q(Py) (Å)	0.015	0.030	−0.101	−0.085
Ph−Py (Å)	1.380	1.364	1.462	1.451
ϕ (°)	−0.1	−0.1	26.0	0.6
ψ (°)	−0.3	−0.1	−4.6	0.0
θ (°)	0.0	0.0	4.4	−0.3
μ (D)	1.75	0.27	−9.61	−12.06

[a] Geometries optimized at the SA-CASSCF level, dipoles calculated at the CASPT2(0.00) level. The negative sign in the dipole indicates the negative charge is displaced toward the phenyl ring. [b] Q′(Ph).

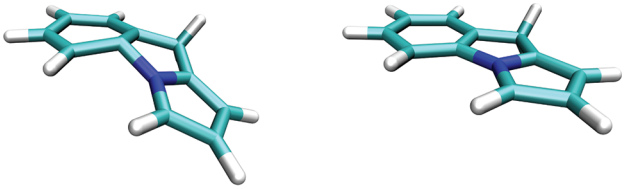

BQ LQ

Figure 5. Perspective view of the two optimized ICT structures in acetonitrile.

Table 6. Vertical Absorption Energies (in eV), Dipole Moments (in D), and Oscillator Strengths for the FPP Molecule in Acetonitrile at the GS Geometry

	vertical energies			
	CASPT2	expt[18]	μ	f
S_0			1.76	
S_1	4.31	4.26	0.82	0.011
S_2	4.75	4.73	−2.55	0.291
S_3	5.28		−5.29	0.031
S_4	5.41		−7.66	0.142

3.2. Acetonitrile Solution. *3.2.1. Optimized Geometries.* The different electronic states obtained in the gas phase for the FPP molecule were also optimized in acetonitrile solution, using the ASEP/MD method[25−27] to model the solvation process. The resulting geometries are given in Table 5. The changes in the geometry are small in all cases, and practically negligible for GS and LE. In the BQ structure the most significant change between the gas phase and acetonitrile is the lengthening of the Ph−Py bond and a slight planarization of the ϕ angle. As expected in a polar solvent, dipole moments are enhanced, only slightly in GS and LE, and more significantly in BQ.

In addition to the minima already described, in solution it was possible to find another minimum in the S_1 surface with ICT character. This minimum is characterized by a planar structure (ϕ, ψ, and θ angles close to zero) and a quinoidal phenyl ring (with two opposite bonds shorter than the other four), and therefore we name it linear quinoidal (LQ). It is interesting that

Table 7. Vertical Emission Energies (transitions to S_0, in eV), Dipole Moments (in D), and oscillator Strengths for the FPP Molecule in Acetonitrile[a]

	vertical energies				
	CASPT2	expt[18]	μ	f	ΔG
LE (S_1)	3.94	3.94	0.27	0.014	4.06
BQ (S_1)	2.70		−9.60	0.003	4.36
LQ (S_1)	3.31	3.29	−12.06	0.003	4.46

[a] ΔG is the relative free energy (in eV) with respect to the ground-state minimum, GS.

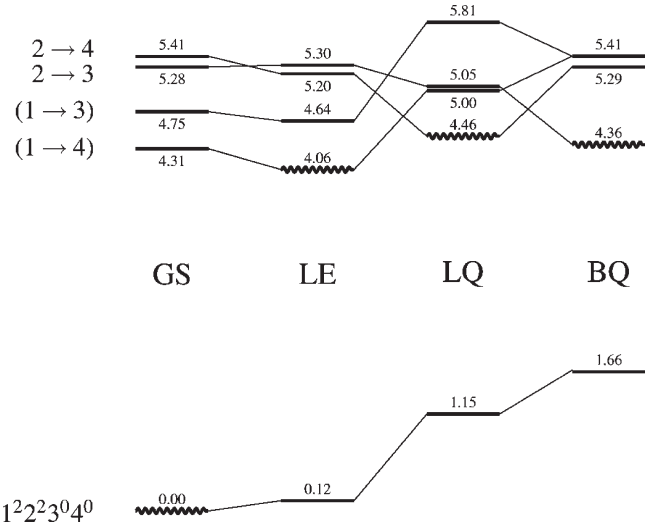

Figure 6. Relative free energies (CASPT2(0.00), in eV) of the calculated electronic states of FPP in acetonitrile solution at the optimized geometries. The state for which each geometry is optimized is marked as a wavy line, this is also the state with which the solvent is in equilibrium. States of equivalent electron configuration are joined by lines. For the nature of the different states, labeled on the left, refer to Table 6 and Figure 3.

in this LQ structure the phenyl deformation does not happen along the $C_{10}-C_{11}$ bond but along the $C_{11}-C_6$ bond, so that it is best described with Q′(Ph) instead of Q(Ph) (see Table 1). The dipole moment of this structure is even larger than for BQ, and it can be noted that the dipole moments of the GS, LE, and LQ structures are in very good agreement with the experimental estimations[17] (1.7 D for the ground state, 1 D for the LE state, and −13 D for the ICT state). The two structures BQ and LQ are compared in Figure 5.

3.2.2. Absorption. The calculated absorption properties of FPP in acetonitrile are summarized in Table 6. All values are very close to the gas phase results, which is not surprising given the weak dipole moment of the ground state and the negligible change in the optimized GS geometry. In the two lowest transitions, a small blue shift is predicted, in accordance with the change of dipole moment between the states. This small blue shift is also observed experimentally when the absorptions in *n*-hexane and acetonitrile solutions are compared.[18]

3.2.3. Fluorescence. The results for the excited state emission properties from the different optimized structures of FPP in solution are shown in Table 7. Similarly to what was found for the absorptions, there is very little change in the LE emission from

the gas phase to acetonitrile, this is consistent with the experiments, where the LE fluorescence band shows practically no solvatochromic shift from *n*-hexane to acetonitrile[18]

The two optimized ICT structures have very different emission energies, with the value for LQ being 0.6 eV larger than for BQ. The observed red-shifted band of FPP in acetonitrile is centered at around 3.29 eV, which is in excellent agreement with the predicted LQ emission. On the basis of the fluorescence energies, the BQ structure can be ruled out as the main source of the ICT band. The relative free energy of the states is listed in the ΔG column, where it can be seen that the difference in free energy between BQ and LQ is small (0.1 eV or 2.3 kcal/mol), and LE is around 0.3 eV (7 kcal/mol) below BQ. All three states are below the absorption Franck−Condon energy (S_2 at GS). A scheme of the energies of the first five states at each structure is shown in Figure 6. Due to the different phenyl deformation in LQ, the equivalence between the states (the lines joining the horizontal lines) is only partial, and there is considerable mixture.

In a theoretical study of PP and FPP, using the polarizable continuum model (PCM) method to include solvent effects, Xu et al.[23] also found that the free energy difference between the ICT structures of FPP is relatively small. In agreement with our results, they obtained a significantly lower fluorescence energy for BQ than for a planar (symmetry-constrained) structure. However, the solvatochromic shift given by PCM is much weaker than ours (0.26 eV vs 0.59 eV for BQ), which leads them to conclude that the emission from BQ in acetonitrile is more similar to the observed ICT band, while the emission from the planar structure would be indistinguishable from the LE emission. In contrast, the fluorescence energies reported in this work indicate that BQ emission is too low to correspond to the experimental band, while the emission from the planar LQ structure is a much better candidate. The difference between our results and those of Xu et al. can be attributed to the absence of specific solute−solvent interactions in PCM and to the different active spaces used in both works.

Druzhinin et al. have estimated some thermodynamic quantities for the FPP system from the fluorescence properties;[18] in particular, from their data it can be concluded that the free energy difference between the emitting LE and ICT states is around 1 kcal/mol in acetonitrile at room temperature. Our results yield the two candidate ICT states about 8 kcal/mol higher in energy than the LE state. Here we must recall that we are using CASPT2(0.00) values in this discussion because they make comparison of electron transition energies with experiments easier. As we indicated previously, transition energies with CASPT2(0.25) are 0.4 to 0.5 eV larger, but the relative stability of the different excited states does not change much. Nevertheless if we take CASPT2(0.25) values, then LE is only around 0.2 eV (4 kcal/mol) below BQ, the free energy difference between LQ and BQ is lower than 2 kcal/mol, and both ICT states lie very close to the S_1 state at GS. Considering the errors, approximations and assumptions in the experiments, interpretations, and calculations, there is qualitative agreement with the recent experimental findings.

If, as we propose, the experimental ICT band corresponds to emission from the LQ structure, there must be a reason why the BQ structure is not formed or its fluorescence is not observed. Since, as seen in Figure 6 and Table 7, the free energies of LQ and BQ, and the oscillator strengths for their vertical emissions are very close, it can be interesting to analyze which ICT structure is reached first during the solute relaxation after the initial absorption. The structural similarity between GS and LQ suggests that

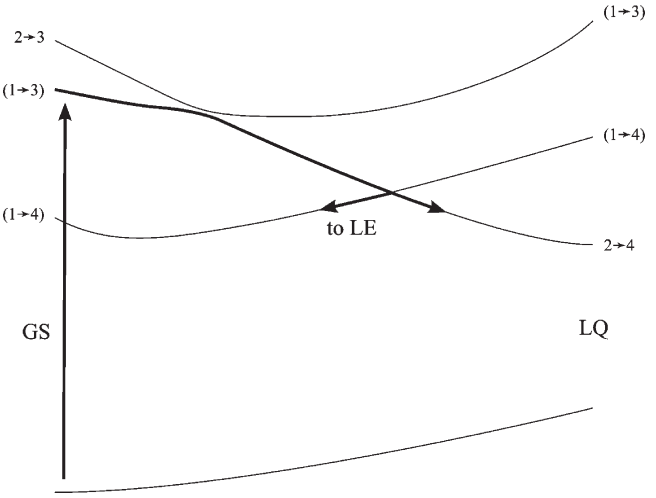

Figure 7. Qualitative scheme of the excited-state optimization of FPP in acetonitrile, starting from the Franck−Condon absorption at the GS structure. The electronic surfaces are labeled as in Figure 6. The bold lines and arrows indicate the path followed by the solute wave function.

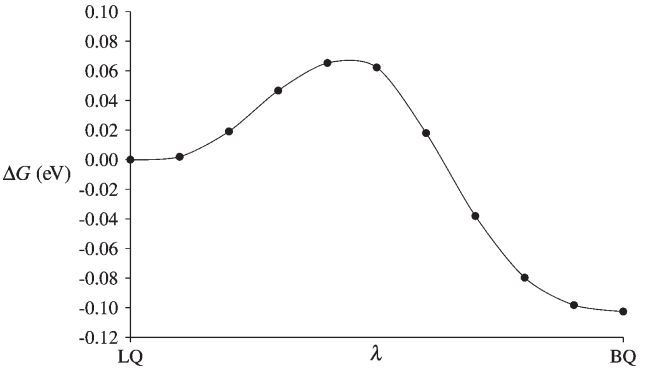

Figure 8. Free energy profile for a geometry interpolation (λ parameter) between the LQ and BQ structures, in acetonitrile.

relaxation leads to LQ first, but a complete description of the process would require a study of the coupled dynamics of solute and solvent, which is beyond the scope of this work. However, within the mean field approximation of ASEP/MD, we can get a qualitative picture by following the gradient during the solute geometry optimization. We did this, optimizing the solute geometry starting with the S_2 state at the GS geometry (Franck−Condon absorption) and observed that the solute structure tends to LQ. The process followed corresponds to that pictured in Figure 7, where there is initially a crossing between the surfaces of S_2 and S_3 and a change in the wave function nature occurs, such that after the crossing there is a clear ICT character in the S_2 surface. Afterward, there is an intersection between the electronic surfaces corresponding to the LE and LQ states; after this intersection, the solute can proceed to either the LQ or LE structures, depending on which surface is followed, which would be determined by the system dynamics.

Once the LQ structure has been reached, there must be some barrier preventing the interconversion between LQ and BQ. We tried to estimate this barrier by performing a FEP calculation between the two ICT structures. The solute geometry was interpolated (in internal coordinates) in 10 steps between LQ

Table 8. Main Experimental and Calculated Excited-State Absorption Bands of FPP (in eV)[a]

expt[18]			
n-hexane	1.50	2.92	
acetonitrile	1.55	2.05	3.40
MS-CASPT2, gas phase			
LE	1.58 (0.149)		3.39 (0.011)
BQ	2.97 (0.008)		3.32 (0.094)
MS-CASPT2, acetonitrile			
LE	1.56 (0.126)		2.24 (0.027)
BQ	2.91 (0.008)		3.17 (0.044)
LQ	2.31 (0.011)		3.75 (0.034)

[a] Oscillator strength is in parentheses.

and BQ, and at each step, the solute wave function and the solvent were equilibrated. The resulting free energy profile (see Figure 8) shows a barrier of around 0.1 eV (2 kcal/mol) in the direction LQ→ BQ. This value is only an upper bound for the barrier in equilibrium conditions, because the path followed is not optimized. The low value obtained for the barrier indicates that dynamical effects are probably important, and therefore further investigations are needed to elucidate the reasons why apparently no emission from BQ is observed experimentally.

It is interesting to compare the results obtained for FPP with those for the related PP.[24] In both systems we find an LQ ICT state, with a fluorescence energy matching the observed spectrum, and other bent structures (BQ) close in energy but with a predicted emission that is too low for the experimental band. These similarities between the two molecules can explain the parallels in their photophysical behavior. In the case of PP, a perpendicular state (PQ) was also found to be possible, which could be a route to nonradiative deactivation, thus decreasing the relative intensity of the ICT emission when compared to FPP, where this PQ structure is not available.

3.3. Excited-State Absorption. Druzhinin et al. have also measured the transient absorption spectra of FPP in *n*-hexane and acetonitrile[18] at different delay times, which has allowed them to assign certain absorption bands to the emitting states responsible for the two fluorescence bands. We have calculated the absorption energies from S_1 to higher excited states at the different optimized structures, with the goal of confirming the nature of the emitting states and their identity with the states probed in the transient absorption. For these calculations we had to include a larger number of states in the CASSCF state averaging (ten in total), and the multistate variant of CASPT2 was needed to separate the electronic states.[44]

The results are summarized in Table 8. Experimentally, the excited state absorption (ESA) spectrum of FPP in *n*-hexane is dominated by a band at 1.50 eV, with a minor band at 2.92 eV, which are attributed to the LE state, since this is the only state observed in the fluorescence spectrum. In acetonitrile, the band at 1.55 eV decreases over the first few ps, while the band at 3.40 eV increases and is therefore assigned to the ICT state.

The most intense absorption predicted by the present calculations occurs at around 1.58 eV, for the LE structure, and changes very little from the gas phase to acetonitrile. This value can be compared with the 1.50 and 1.55 eV bands observed in the experiments, confirming that the LE state can be the source of these bands. The other absorption found in *n*-hexane should also correspond to the LE state, but to adequately reproduce it in the calculations, a higher number of states would probably be needed (the ninth root is still only 2.7 eV above S_1).

For the ICT structures in acetonitrile solution, BQ, and LQ, we do not find any absorption of similar intensity, all oscillator strengths being significantly lower. This somewhat agrees with the ESA spectrum measured at longer delay times, which is relatively weak. The experimental band at 3.40 lies approximately between the two most intense absorptions predicted, at 3.17 and 3.40 eV. It can be tempting to assign the experimental band to either of the two predicted transitions (or a combination thereof), but both theoretical values correspond to high excited states and are therefore subject to significant errors. The fact is that the present results do not allow an inequivocal determination of the origin of the ESA spectrum of FPP in acetonitrile at long delays.

4. CONCLUSIONS

We have studied the ground and excited singlet states of fluorazene in the gas phase and in acetonitrile solution, using a high-level quantum method for the electronic structure and an explicit mean-field MM model for the solvent. The optimized structures for the GS and the LE state provide good agreement with the observed absorption bands and the higher-energy fluorescence band. These states are characterized by very low dipole moments and are only weakly affected by the solvent; in consequence, their photophysic properties show little change between the gas phase and solution. The agreement between the computed results for the LE state and the emission and excited-state absorption properties in *n*-hexane indicates that this state is adequately described by the present theoretical methods, and there is, in our opinion, little doubt on its nature and participation in the dual fluorescence of FPP.

The situation is less clear for the ICT state, responsible of the lower-energy fluorescence band. In the gas phase only a minimum is located, and this state is 0.5 eV higher in energy than the LE state. In acetonitrile solution we obtain two optimized structures for states of significant charge-transfer character, both structures being similar in energy. In one of these structures, LQ, the molecule skeleton is kept planar, and its emission energy and dipole moment are in good agreement with the experimental band, while in the other, BQ, the C_6 atom is pyramidalized, and its emission energy is around 0.6 eV lower. Our results therefore suggest that the experimental ICT fluorescence originates from LQ.

The excited-state absorption calculations for the different structures confirm the LE state as responsible for the 800 nm band, but they do not allow a conclusive assignment for the ICT signals.

Finally, why emission from BQ is not experimentally registered remains an open question, and to arrive to a definitive conclusion, possibly more sophisticated and accurate electronic structure methods are needed, along with the inclusion of further effects not considered in this work, such as the excited-state dynamics or vibronic coupling. With the current results, however, we can state that the twist between the electron-donor and -acceptor groups is not necessary for an ICT state to be stabilized.

AUTHOR INFORMATION

Corresponding Author
*E-mail: jellby@unex.es.

■ ACKNOWLEDGMENT

This work was supported by the CTQ2008-06224/BQU Project from the Ministerio de Ciencia e Innovación of Spain, co-financed by the European Regional Development Fund (ERDF), and the PRI08A056 Project from the Consejería de Economía, Comercio e Innovación of the Junta de Extremadura. I.F.G. acknowledges the Junta de Extremadura and the European Social Fund for financial support, and A.M.L. acknowledges financial support from the Juan de la Cierva subprogramme of the Ministerio de Ciencia e Innovación of Spain. The authors also thank the Fundación Computacióny Tecnologóas Avanzadas de Extremadura (COMPUTAEX) for additional computational resources.

■ REFERENCES

(1) Lippert, E.; Lüder, W.; Moll, F.; Nägele, W.; Boos, H.; Prigge, H.; Seibold-Blankenstein, I. *Angew. Chem.* **1961**, *73*, 695–706.
(2) Grabowski, Z. R.; Rotkiewicz, K.; Rettig, W. *Chem. Rev.* **2003**, *103*, 3899–4032.
(3) Herbich, J.; Pérez Salgado, F.; Rettschnick, R. P. H.; Grabowski, Z. R.; Wojtowicz, H. *J. Phys. Chem.* **1991**, *95*, 3491–3497.
(4) Peng, L. W.; Dantus, M.; Zewail, A. H.; Kemnitz, K.; Hicks, J. M.; Eisenthal, K. B. *J. Phys. Chem.* **1987**, *91*, 6162–6167.
(5) Lommatzsch, U.; Gerlach, A.; Lahmann, C.; Brutschy, B. *J. Phys. Chem. A* **1998**, *102*, 6421–6435.
(6) Chudoba, C.; Kummrow, A.; Dreyer, J.; Stenger, J.; Nibbering, E. T. J.; Elsaesser, T.; Zachariasse, K. A. *Chem. Phys. Lett.* **1999**, *309*, 357–363.
(7) Druzhinin, S. I.; Demeter, A.; Galievsky, V. A.; Yoshihara, T.; Zachariasse, K. A. *J. Phys. Chem. A* **2003**, *107*, 8075–8085.
(8) Druzhinin, S. I.; Mayer, P.; Stalke, D.; von Blow, R.; Noltemeyer, M.; Zachariasse, K. A. *J. Am. Chem. Soc.* **2010**, *132*, 7730.
(9) Kato, S.; Amatatsu, Y. *J. Chem. Phys.* **1990**, *92*, 7241–7257.
(10) Hayashi, S.; Ando, K.; Kato, S. *J. Phys. Chem.* **1995**, *99*, 955–964.
(11) Serrano-Andrés, L.; Merchán, M.; Roos, B. O.; Lindh, R. *J. Am. Chem. Soc.* **1995**, *117*, 3189–3204.
(12) Sudholt, W.; Arnulf Staib, A. L. S.; Domcke, W. *Phys. Chem. Chem. Phys.* **2000**, *2*, 4341–4353.
(13) Mennucci, B.; Toniolo, A.; Tomasi, J. *J. Am. Chem. Soc.* **2000**, *122*, 10621–10630.
(14) Rappoport, D.; Furche, F. *J. Am. Chem. Soc.* **2004**, *126*, 1277–1284.
(15) Minezawa, N.; Kato, S. *J. Phys. Chem. A* **2005**, *109*, 5445–5453.
(16) Gómez, I.; Mercier, Y.; Reguero, M. *J. Phys. Chem. A* **2006**, *110*, 11455–11461.
(17) Yoshihara, T.; Druzhinin, S. I.; Zachariasse, K. A. *J. Am. Chem. Soc.* **2004**, *126*, 8535–8539.
(18) Druzhinin, S. I.; Kovalenko, S. A.; Senyushkina, T. A.; Demeter, A.; Zachariasse, K. A. *J. Phys. Chem. A* **2010**, *114*, 1621–1632.
(19) Parusel, A. B. J. *Phys. Chem. Chem. Phys.* **2000**, *2*, 5545–5552.
(20) Proppe, B.; Merchán, M.; Serrano-Andrés, L. *J. Phys. Chem. A* **2000**, *104*, 1608–1616.
(21) Zilberg, S.; Haas, Y. *J. Phys. Chem. A* **2002**, *106*, 1–11.
(22) Schweke, D.; Baumgarten, H.; Haas, Y.; Rettig, W.; Dick, B. *J. Phys. Chem. A* **2005**, *109*, 576–585.
(23) Xu, X.; Cao, Z.; Zhang, Q. *J. Phys. Chem. A* **2006**, *110*, 1740–1748.
(24) Fdez. Galván, I.; Martín, M. E.; Muñoz-Losa, A.; Sánchez, M. L.; Aguilar, M. A. *J. Chem. Theory Comput.* **2011**, *7*, 1850–1857.
(25) Sánchez, M. L.; Aguilar, M. A.; Olivares del Valle, F. J. *J. Comput. Chem.* **1997**, *18*, 313–322.
(26) Fdez. Galván, I.; Sánchez, M. L.; Martín, M. E.; Olivares del Valle, F. J.; Aguilar, M. A. *Comput. Phys. Commun.* **2003**, *155*, 244–259.
(27) Aguilar, M. A.; Sánchez, M. L.; Martín, M. E.; Fdez. Galván, I. An Effective Hamiltonian Method from Simulations: ASEP/MD . In *Continuum Solvation Models in Chemical Physics*, 1st ed.; Mennucci, B., Cammi, R., Eds. Wiley: Hoboken, NJ, 2007; Chapter 4.5, pp 580−592.
(28) Fdez. Galván, I.; Sánchez, M. L.; Martín, M. E.; Olivares del Valle, F. J.; Aguilar, M. A. *J. Chem. Phys.* **2003**, *118*, 255–263.
(29) Okuyama-Yoshida, N.; Nagaoka, M.; Yamabe, T. *Int. J. Quantum Chem.* **1998**, *70*, 95–103.
(30) Zwanzig, R. W. *J. Chem. Phys.* **1954**, *22*, 1420–1426.
(31) Fdez. Galván, I.; Aguilar, M. A.; Ruiz-López, M. F. *J. Phys. Chem. B* **2005**, *109*, 23024–23030.
(32) Roos, B. O.; Taylor, P. R.; Siegbahn, P. E. M. *Chem. Phys.* **1980**, *48*, 157–173.
(33) Andersson, K.; Malmqvist, P.-Å.; Roos, B. O.; Sadlej, A. J.; Wolinski, K. *J. Phys. Chem.* **1990**, *94*, 5483–5488.
(34) Andersson, K.; Malmqvist, P.-Å.; Roos, B. O. *J. Chem. Phys.* **1992**, *96*, 1218–1226.
(35) Ghigo, G.; Roos, B. O.; Malmqvist, P.-Å. *Chem. Phys. Lett.* **2004**, *396*, 142–149.
(36) Jorgensen, W. L.; Maxwell, D. S.; Tirado-Rives, J. *J. Am. Chem. Soc.* **1996**, *118*, 11225–11236.
(37) Aquilante, F.; De Vico, L.; Ferré, N.; Ghigo, G.; Malmqvist, P.-Å.; Neogrády, P.; Pedersen, T. B.; PitoYák, M.; Reiher, M.; Roos, B. O.; Serrano-Andrés, L.; Urban, M.; Veryazov, V.; Lindh, R. *J. Comput. Chem.* **2010**, *31*, 224–247.
(38) Refson, K. *Comput. Phys. Commun.* **2000**, *126*, 310–329.
(39) Schaftenaar, G.; Noordik, J. H. *J. Comput.-Aided Mol. Des.* **2000**, *14*, 123–134.
(40) He, R.-X.; Li, X.-Y. *Chem. Phys.* **2007**, *332*, 325–335.
(41) Fdez. Galván, I.; Martín, M. E.; Muñoz-Losa, A.; Aguilar, M. A. *J. Chem. Theory Comput.* **2009**, *5*, 341–349.
(42) Valsson, O.; Filippi, C. *J. Chem. Theory Comput.* **2010**, *6*, 1275–1292.
(43) Fdez. Galván, I.; Martín, M. E.; Aguilar, M. A. *J. Chem. Theory Comput.* **2010**, *6*, 2445–2454.
(44) Finley, J.; Malmqvist, P.-Å.; Roos, B. O.; Serrano-Andrés, L. *Chem. Phys. Lett.* **1998**, *288*, 299–306.